Omnidirectional flexural invisibility of multiple interacting voids in vibrating elastic plates

D. Misseroni[1], A.B. Movchan[2], D. Bigoni[1,*]

SUPPLEMENTARY MATERIAL

[1] *DICAM, University of Trento, via Mesiano 77, I-38123 Trento, Italy.*
[2] *Department of Mathematical Sciences, University of Liverpool, Liverpool L69 3BX, UK.*
*E-mail: davide.bigoni@unitn.it

Keywords: Cloaking, Structured plates, waves, scattering reduction.

1   The-state-of-the art on cloaking, with special reference to elasticity

The state-of-the-art on cloaking (particularly addressed to elasticity) is presented with respect to the following definition of invisibility requirements:

- (i.) easiness of coating implementation technology;

- (ii.) smallness of the ratio between the thickness of coating skin and the dimensions of the object to be made invisible;

- (iii.) smallness of ratio between the dimensions of object to be made invisible and of the hosting medium;

- (iv.) overall scattering suppression;

- (v.) broad bandwidth;

- (vi.) multidirectionality;

- (vii.) invisibility of multiple coated objects.

- (i.) Cloaking has always been related to the use of (in the words of the authors of the papers referenced below) 'exotic materials'. In *electromagnetism*, concepts from transformation optics imply spatially inhomogeneous and anisotropic magnetic and dielectric tensors. At the same time, no reflection should be produced at the cloaking interface and superluminal propagation with extreme values of the constitutive parameters have to be attained in the cloak. In *acoustics*, a partial coating of a sphere of 4 cm in radius was obtained using 60 concentric acoustically rigid tori[1]. In *elasticity*: pentamode[2], Cosserat[4, 3], anisotropic density[5], prestressed[6], nonlinearly prestrained[7] materials, or application of in-plane body forces[8, 9] have been proposed for the cloaking, all mechanical set-ups posing formidable difficulties of implementation. For flexural waves at least 10 concentric layers made up of six different materials were proposed to obtain cloaking[10], so that in an experimental realization of this proposal, 20 concentric rings and 16 different elastic metamaterials were used[11], only to achieve an approximation to cloaking. The complexity of all systems so far proposed rather demonstrates impossibility than possibility of cloaking.

- (ii.) The importance of small thickness for the cloaking skin was pointed out, together with the indication of a route to ultrathin coating, in optics[12]. The ratio between the thickness of the coating skin and the dimension of the coated object is 0.6 in a paper devoted to acoustic[1], while in elasticity, for quasi-static behaviour, the coating ratio is 0.17 for an approximate, unidirectional, and quasi-static cloaking[13], 0.41 for a cloaking in a lattice material[14]. For out-of-plane elastic waves, the coating is infinite (thus representing all the medium where the waves propagate) for nonlinearly strained solids[15, 16, 7], it is 3 for a nonlinear flexural cloak[17], while the thickness ratio is 0.5 for an approximate cloaking in a discrete lattice structure[18]. Finally, for flexural waves the thickness ratio is 1.5[11] and 0.5[19] in the few papers where experiments are reported, while the ratio becomes 5 and 1.6[8] (note that the cloak is much less effective for the latter values than for the former), 1.17[10], and 0.5[9, 20, 6] in theoretical models involving flexural waves.

- (iii.) The ratio between the dimensions of the hosting medium and of the coated object is often assumed to be infinite in theoretical considerations and realized as large in the experiments. However, this ratio should be kept as small as possible, to reveal that the coated object is more than a mere perturbation to a large field. In elasticity, the ratio is *infinite* in theoretical papers, where an infinite hosting medium is almost always considered[15, 16, 7, 5, 18, 8, 20, 10, 9, 6, 14]. In experimental papers, the situation is different, so that the ratio goes down to 4.3 for quasi-static cloaking[13] and to 5 [19] and 8 [17] for flexural waves. This ratio is unfortunately not reported for experiments and is again assumed null in the simulations relative to an approximate flexural cloak[11].

- (iv.) Obviously, the chief characteristic of cloaking is overall scattering suppression, a condition which is usually reached only in an approximate sense. At sub-wavelengths, more than 15 dB in scattering reduction is observed for a mantle cloak [21], while in acoustics 90% of maximum scattering is experimentally obtained at 8.55 kHz, but this reduces to 70% for larger bandwidth [1]. Quantitative data on scattering reduction are often not explicitly reported in elasticity [8, 20, 10, 9, 6] and the experiments are no exception to this rule [11], although a performance of 60% for a cloak was reported in terms of coefficients of the Fourier expansion for the scattered field[19] and a performance of 55% was reported for a nonlinear cloak [17]. In elasticity, not only perfect scattering reduction has never been achieved even at a single frequency, but usually, the scattering reduction is low.

- (v.) Invisibility should be achieved for a wide band of wavelengths. The first experimental demonstration of microwave cloaking [22] was obtained at the specific frequency of 8.5 GHz and only later extended to cover the narrow range of 13-16 Hz[23], while a broadband response was obtained only at the sacrifice of omnidirectionality[24]. In acoustics, the broadband requirement is difficult to be achieved, so that, even restricting the cloak to unidirectional waves, a 90% of scattering was obtained only at 8.55 kHz, while the performance of the cloaking fell down already at the very closed frequency of 8.62 kHz[1]. Interestingly, by reducing the requirement of scattering cancellation down to a minimum of 70% the cloak bandwidth was 120 Hz. In any case, by Kramers-Kronig-like dispersion relations limits the bandwidth over which passive linear acoustic materials can work.

The situation in elasticity is much worse than in electromagnetism, due to the vectorial nature of the wave propagation. In planar elasticity under antiplane shearing (which introduces a strong simplification), the requirement of invisibility was restricted to a given frequency[25], or only partial cloaking was achieved[7], or cloaking was only working for wavelengths of the same order

of the dimension of the cloaked object[26], or 25 times the maximum cell size in the latticed cloak[2].

A series of papers devoted to invisibility for flexurally vibrating thin plates report more or less approximate cloakings *only* for certain frequencies (40 Hz[4], but the cloak is declared not to work at 200 Hz, 314 and 157 rad/s[9], not declared[20, 27] at wavenumbers 3, 5, and 10[18], for wavenumbers ranging between 15-22.5[10], at 90, 120, 180, 210, 230 Hz[19] at a wavelength 0.42[10]). A broadband cloaking with an efficiency ranging between -160% and 55% was reported on within a high frequency range (2-11 kHz [17]). It can be finally mentioned that the model of plate vibration has been used to investigate earthquake shielding systems[28, 29]. Here a partial cloaking was obtained for a frequency of 50 Hz[28] and of 4.5 Hz (the frequency range was improved to work up to 26 Hz adopting an invasive reinforcement)[29]. With a different cloaking system, Rayleigh and bulk waves have been attenuated in the range 1-10 Hz[30]. As a matter of fact, data on cloak performances are never reported for a continuous spectrum of frequencies.

- (vi.) Ideally, invisibility should concern waves coming from every direction (emanating from a punctual source, reflected from boundaries, interacting with non-invisible objects). For electromagnetic waves invisibility for unidirectional waves without phase preservation is trivial, so that the challenge is omnidirectional cloaking[21]. However, unidirectionality is often the working framework for microwaves[24] and acoustics[1], while in elasticity the source of the waves if often a pulsating force acting in an infinite medium (so that reflection of the waves against objects or boundaries is excluded)[15, 16, 7, 20, 10, 18, 9]. Some cases are restricted to unidirectionality[8, 19], which is also the situation addressed in the numerical evaluation (the geometry of experiments is not reported) relative to flexural cloak[11].

- (vii.) Neither theoretical nor experimental attempts have been so far reported to render multiple objects invisible. This 'multiple invisibility' is especially important when the objects are located at a relative distance implying a strong interaction between them.

2   The elastic plate

2.1   Experimental

Vibration tests were performed using the electromagnetic actuator System TIRA vib 51144 (Frequency range 2-6500 Hz, Rated peak force SINE/RANDOM 440N, Max rated travel 25.4mm), equipped with Power Amplifier TIRA BAA 1000 (Frequency range 2-20000 Hz) and mounted on a pneumatic optical table (Nexus Optical Table, from Thorlabs). A stroboscope HD50/LS (Bint, Italy), equipped with two synchronized stroboscopic lights, was used to visualize the deformed shape of the oscillating plate in slow motion. Movies were recorded with a Sony PXW-FS5 video camera and photos were taken with a Sony α9 camera.

The three elastic plates (made up of polycarbonate 3 mm $\times$ 70 mm $\times$ 580 mm), one intact, two perforated with three square voids (each of dimension 45 mm $\times$ 45 mm), one of which with cloaked voids, were produced by cutting a polycarbonate plate with a CNC milling machine (EGX-600, accuracy 0.01 mm, Roland). The mechanical properties of the polycarbonate, namely, the elastic modulus, mass density and Poisson ratio, are respectively $E = 2350$ MPa, $\rho = 1200$ kg/m^3 and $\nu = 0.35$.

The reinforcing of the boundary required to cloak the voids was achieved by gluing two identical thin and square frame elements (one for the intrados and one for the extrados of the plate) around

the boundary of each void of the plate. Each frame, made up of polycarbonate, has a cross-section of 1.148 mm × 5 mm. The redistribution of the mass, removed by drilling the voids, was obtained by gluing 10 concentrated masses (small nuts have been used) of 0.46×10^{-3} kg around each void.

2.2 Finite element simulations

With the purpose of complementing the experiments and to provide more comprehensive results for high frequencies, full 3D ABAQUS finite element simulations were carried out. The three-dimensional systems were designed parametrically in SolidWorks in order to mimic realistic situations. About 250000 second-order tetrahedral elements (C3D10) were employed to discretize each plate. Both the eigenmodes and the steady-state frequency response of each plate were computed. Computational results are reported in Fig. 1a, for the three parallel voids considered in the experiments, in Fig. 1b, for three voids with random inclination, and in Fig. 1c, in the case of seven randomly located and inclined voids.

In all the cases analyzed numerically (to reproduce the conditions used for the experiments) a sinusoidal displacement with null rotation has been imposed on one end of the plate, while all the other ends were left traction-free.

Fig. 1a shows coincidence of the first six vibrational modes for the intact plate and the plate with cloaked voids. Fig. 1b also reveal the multidirectionality of the cloaks, which are now inclined with respect to the direction of the wave propagation. Fig. 1c depicts the omnidirectionality of the cloaks for seven voids randomly located and inclined. Figures (b) and (c) show that for several frequencies the vibrational modes (six are reported) of the intact plate and of the plate with cloaked voids coincide, but are different from those pertinent to the plate (remaining almost undeformed) with unreinforced voids.

2.3 Purely flexural behaviour

If the vibrational motion of the plate is limited to flexural vibrations, the accuracy of the cloak becomes higher. This is shown with the numerical simulations reported in Fig. 2, where the lateral displacement of the plate is prescribed to be purely flexural. The results are presented in terms of scattering reduction, quantified now in terms of displacements (differently from the main article), through the 'scattering reduction coefficient' [1] $(u_z^c - u_z^i)/(u_z^v - u_z^i) \in [0, 1]$, namely, the quotient of the end displacements relative to the cases with cloaked and uncloaked voids, both subtracted from the displacement relative to the intact plate. Therefore, a perfect cloak realizes a coefficient equal 0, while 1 correspond to a completely inefficient one even if values greater than 1 can arise, meaning that the cloak is worse than nothing.

The case in which the voids are parallel to the wave propagation shows a very high scattering reduction, which ranges between $\approx 99.57 \%$ and $\approx 69.54 \%$.

3 The structured plate

3.1 Low frequency range

With reference to boundary conditions of imposed sinusoidal displacements with null rotation on one end, of clamping on the opposite end and traction-free conditions on the remaining ends, computational results are reported in Fig. 3, for frequencies ranging between 20 Hz and 100 Hz. The diagrams in this figure include the color maps of the flexural displacement for: (i.) the intact lattice (without void); (ii.) the lattice with the square void (without reinforcement and mass redistribution); (iii.)
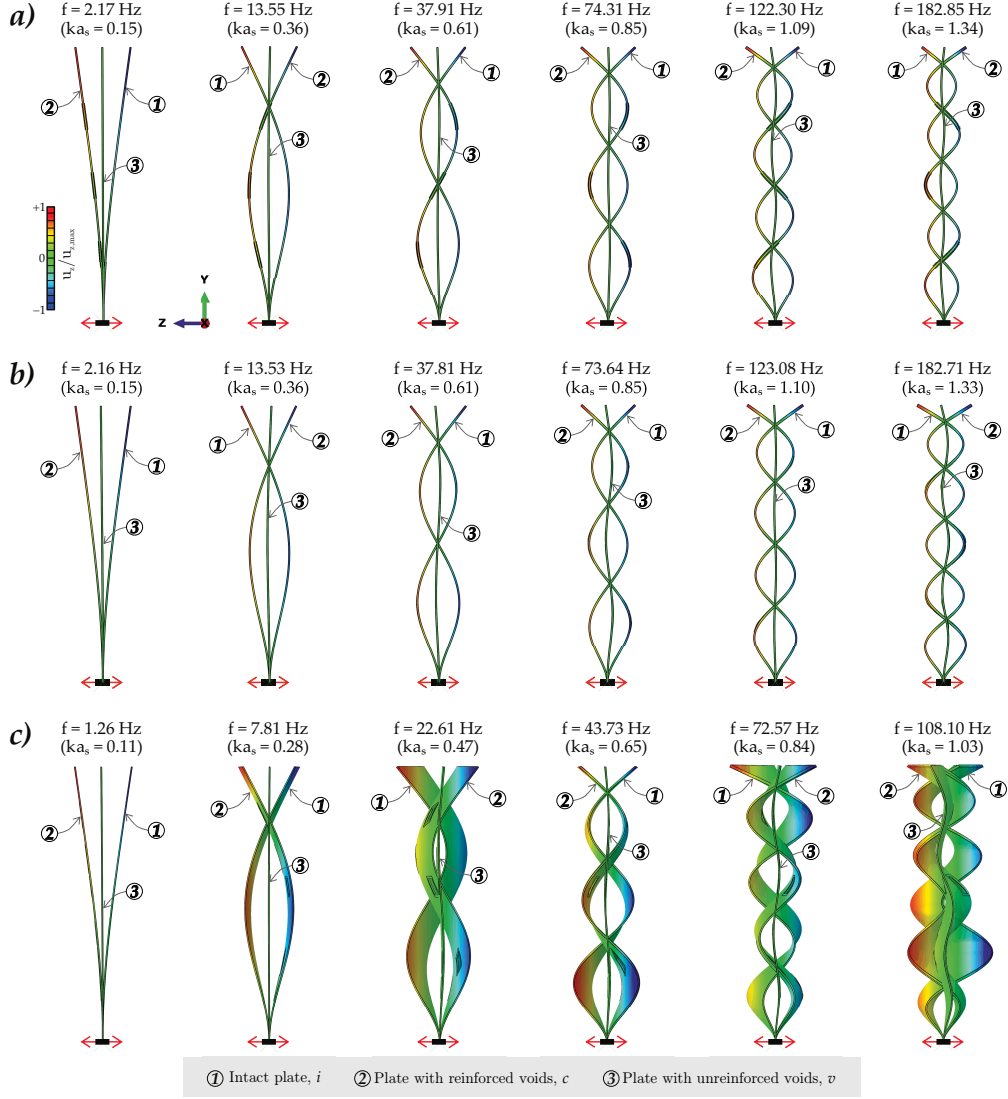
Fig. 1: (a) Invisibility of multiple cloaked voids: the first six vibrational eigenmodes coincide for the intact plate and the plate with cloaked voids and differ from those pertinent to the plate (remaining almost undeformed) with unreinforced voids. (b) Omnidirectionality of invisibility cloak for multiple voids at random inclinations and (c) randomly located and inclined: for several frequencies the vibrational modes (six are shown) coincide for the intact plate and the plate with cloaked voids and differ from those pertinent to the plate (remaining almost undeformed) with unreinforced voids.

the lattice with the square void reinforced through a stiffening boundary layer where the mass is redistributed.

The color maps are accompanied by the diagrams of the amplitudes of the scattered field measured along the circles of the radii 130 mm and 150 mm. In these graphs, the solid lines represent the scattered flexural displacement around the reinforced void, whereas the dashed lines correspond to the scattered flexural displacement around the square void without reinforcement and mass redistribution.

The comparison has to be made between the data evaluated on the circle of the same radius, in particular, data have reported with a blue (red) line for the circle of radius 130 mm (150 mm), see Fig. 5.

It can be observed from Fig. 3 that at low frequency (20 Hz) the presence of the void, reinforced
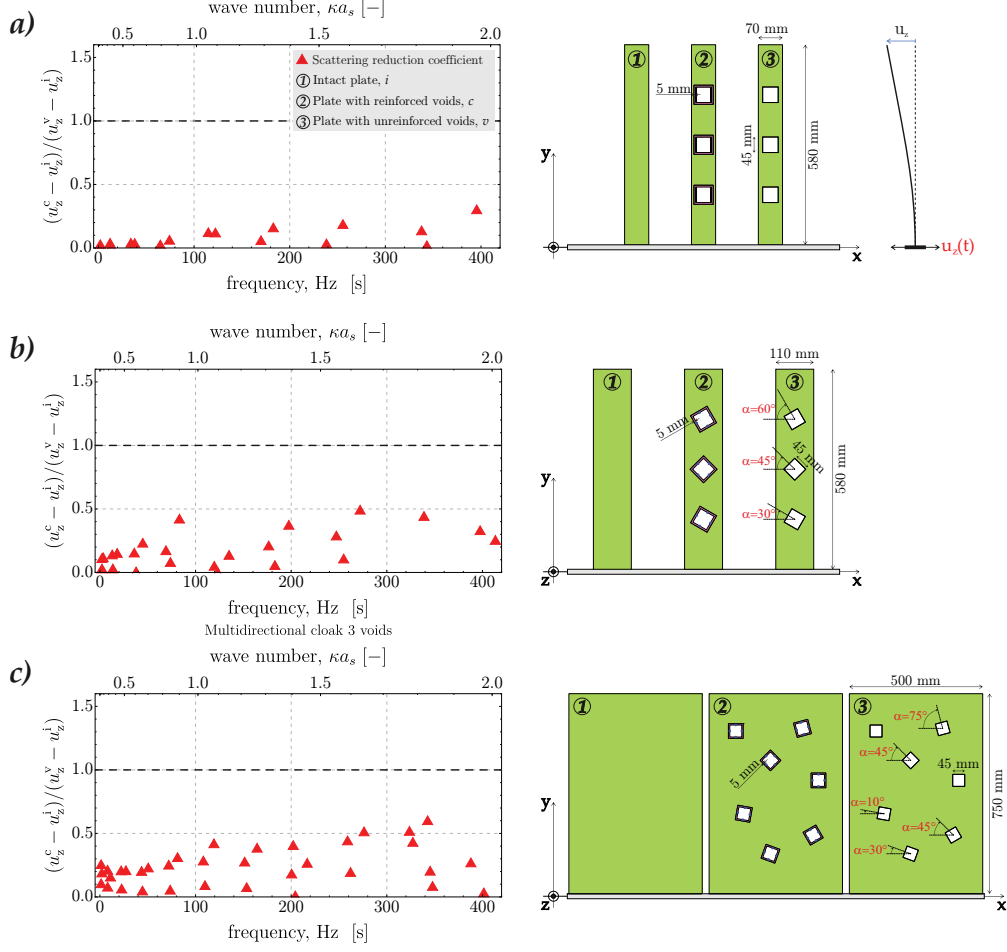
Fig. 2: Purely flexural vibrations of a plate with (a) three parallel voids reinforced as in the experiment; (b) three voids with random inclinations and (c) seven randomly located and oriented voids. In (b) and (c) the cloaking matches bending and torsinal stiffness and the mass distribution matches the second moment of inertia

or not, does not alter much the response. However, the cloaking effect of the reinforcing layer becomes clearly evident starting from the frequency of 40 Hz. At 60 Hz and 80 Hz the cloaking works very well. The wave front in the homogeneous plate is planar and its distortion produced by the presence of the unreinforced void becomes distinctly visible at 80 Hz, but this distortion is strongly reduced in the case of the cloaked void.

For frequencies below 100 Hz, it is consistently demonstrated that the reinforcement and the mass redistribution of the boundary of the square void have led to the reduction of the scattering and to restoring the wave front behind the obstacle.

3.2 High frequency range

Results of computations are shown in Fig. 4, reporting the same fields shown in Fig. 3, but referring now to the high frequency range of 120-200 Hz.

At such frequencies, one would expect that the procedure based on the reinforcement of the boundary and redistribution of the inertia could become less accurate. Nevertheless, a significant reduction of scattering is observed for cloaked void, clearly appreciable when the fields are compared
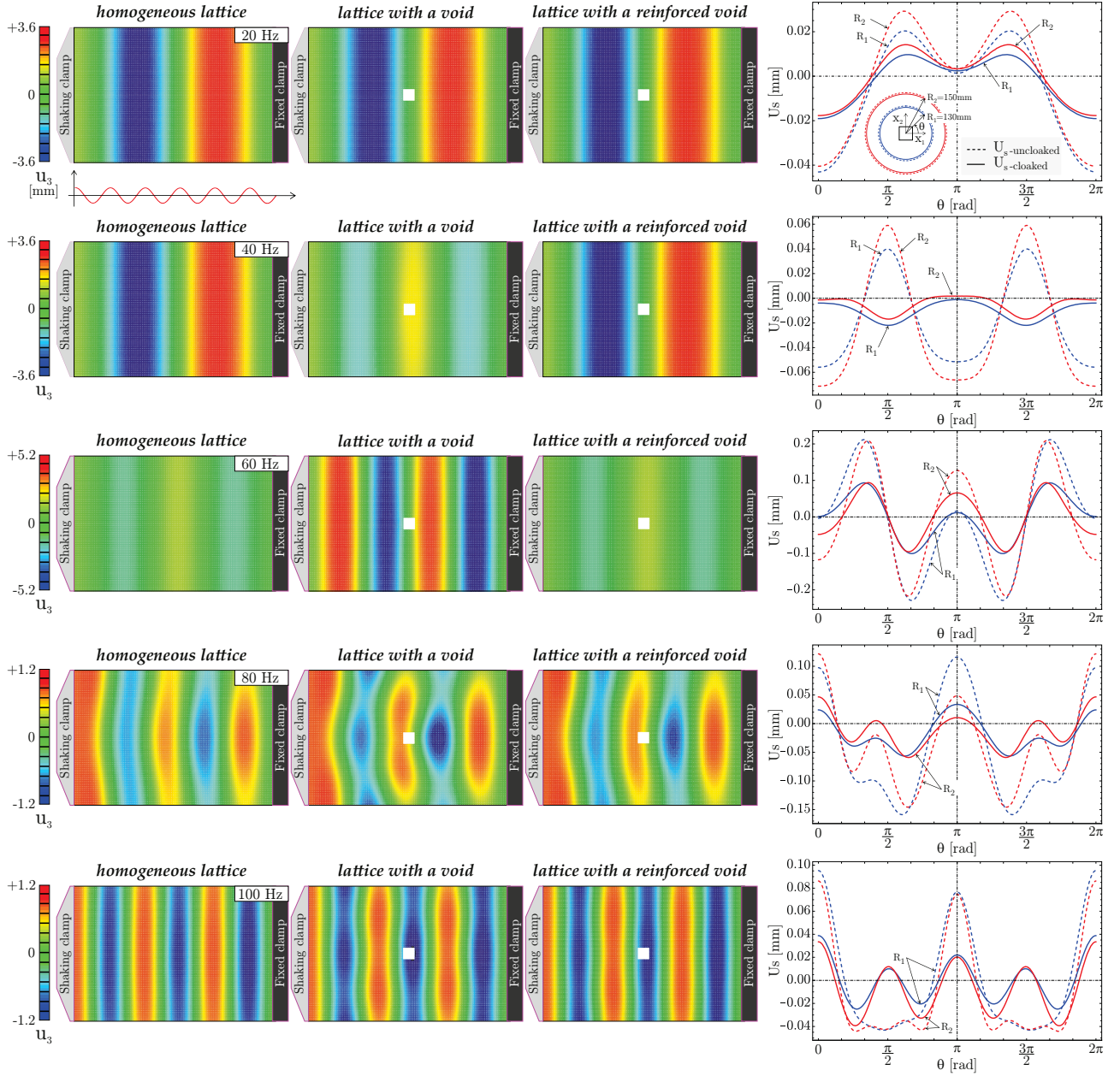
Fig. 3: Flexural out-of-plane displacement distribution (u_3, [mm]) and scattered field U_s at low frequencies evaluated with the finite element program Abaqus, (from left to right) for the uniform lattice, for the lattice with a square void, and for a lattice with cloaked void. The scattered field, evaluated along two concentric circles (blue for radius 130 mm and red for 150 mm, as reported in Fig. 5) for the uniform lattice and for the lattice containing the cloaked square void, is reported on the right.

to those pertinent to the void without reinforcement and mass redistribution. The beneficial effect of the reinforcement is observed up to 200 Hz and beyond (data not reported for brevity).
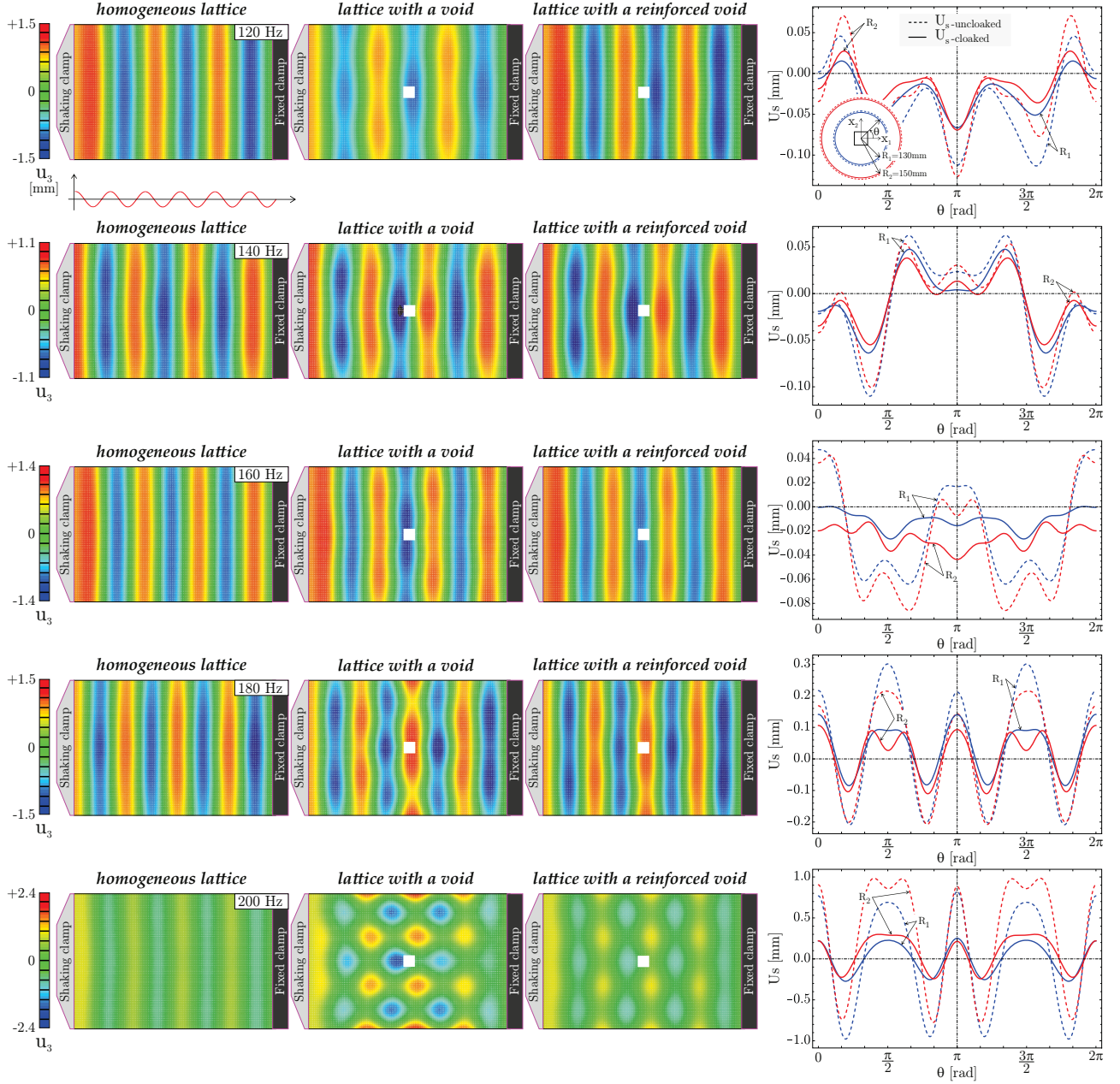
Fig. 4: As for Fig. 3, but at high frequencies ranging between 120 and 200 Hz.

3.3 Evaluation of the multipole coefficients for the scattered field

Quantitative data on scattering reduction can be obtained for a reinforced void, by considering the scattered flexural displacement field u_s, represented along a circle of radius R, concentric to the square void, in the form

$$u_s(R, \theta) = \sum_{i=0}^{N} C_i(R) \cos(i\theta), \tag{1}$$

8

where θ stands for the polar angle, $\theta \in [-\pi, \pi)$, and R is the polar radius. The geometry of the elastic solid and the applied load are symmetric with respect to the horizontal axis, so that the series (1) represents an even function of θ.

The moduli of the Fourier coefficients $|C_i(R_1)|, |C_i(R_2)|, i = 0, ..., 4$, have been evaluated on the data obtained from the numerical simulations for the scattered flexural displacement along the circular paths of radii $R_1 = 130$ mm and $R_2 = 150$ mm, Figs. 5 and 6.

In these diagrams, circular spots are used to mark values corresponding to the Fourier coefficients of the scattered displacement around the square void without reinforcement and mass redistribution, while the triangular markers are used for the 'cloaked' square void (with the reinforced boundary and redistributed mass). Figs. 5 and 6 cover frequencies ranging respectively between 20 and 100 Hz and between 120 and 200 Hz. The index i used in the figures denotes the index of the coefficient in the series (1). The triangular markers always lie below the circular ones, so that results clearly indicate that the computed Fourier coefficients for the cloaked void have moduli remarkably smaller than those pertaining to the uncloaked void.

A direct comparison between different cases is straightforward from Figs. 5 and 6, so that the orders of magnitude of $C_i(R)$ for given frequencies can be appreciated. For example, at 100 Hz the maximum value of coefficients is smaller, approximately by 10 times, than the maximum value at the high frequency of 200 Hz.

The values of the multipole expansion coefficients reported in Figs. 5 and 6 are listed in Tables 1 and 2.
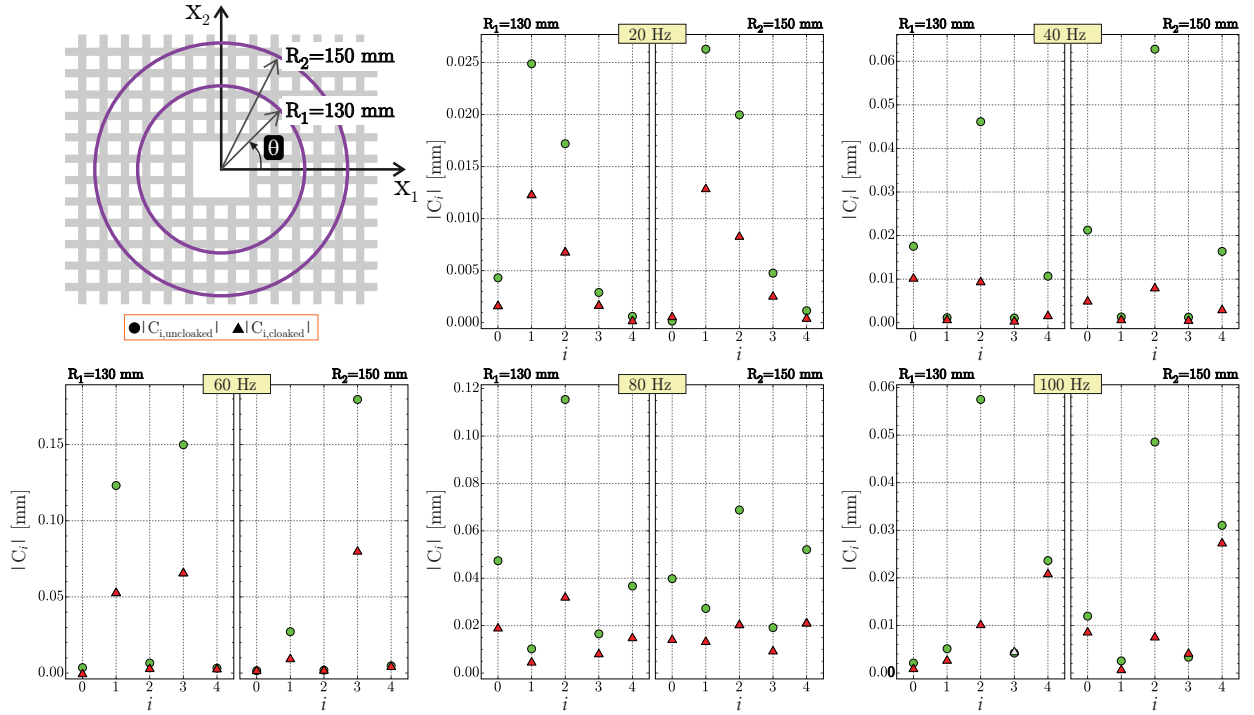
Fig. 5: Fourier coefficients for the representation of the scattered displacement around a square void in a structured plate subject to sinusoidal vibration, note that index i is pertinent to the series (1). Frequencies range between 20 and 100 Hz and coefficients are evaluated with reference to the two circular contours of the radii 130 mm and 150 mm. Results show that the moduli of the Fourier coefficients for the case of the cloaked void are smaller than those referring to the case of uncloaked void.

Fig. 6: As for Fig. 5, but for frequencies ranging between 120 and 200 Hz. Note that even at the high frequency of 200 Hz the scattered field is strongly reduced when reinforcement and mass redistribution is used.
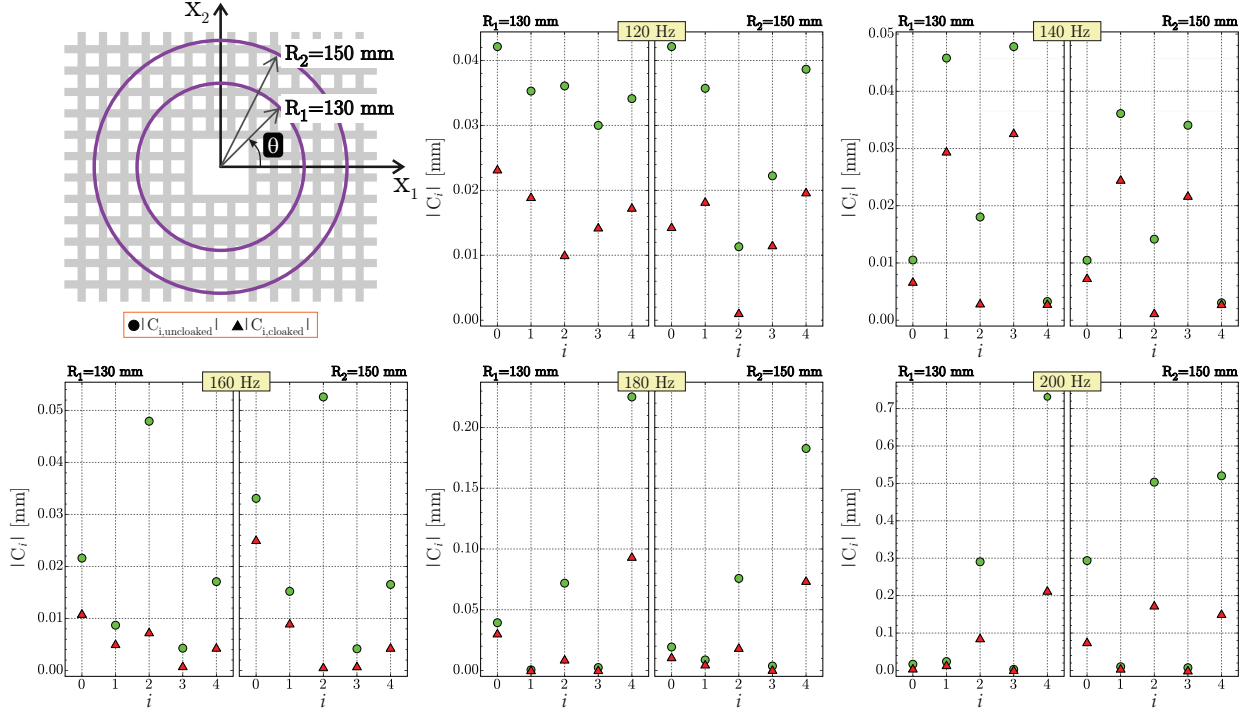
Coeff. $|C_i| \times 10^{-2}$	f_1=20 Hz					f_2=40 Hz				
	C_0	C_1	C_2	C_3	C_4	C_0	C_1	C_2	C_3	C_4
Uncloaked voids	0.432	2.488	1.720	0.291	0.061	1.754	0.115	4.613	0.108	1.068
Cloaked voids	0.172	1.238	0.688	0.175	0.026	1.040	0.087	0.957	0.055	0.179

Coeff. $|C_i| \times 10^{-2}$	f_3=60 Hz					f_4=80 Hz				
	C_0	C_1	C_2	C_3	C_4	C_0	C_1	C_2	C_3	C_4
Uncloaked voids	0.355	12.316	0.654	14.991	0.322	4.738	1.021	11.543	1.654	3.670
Cloaked voids	0.006	5.333	0.344	6.631	0.324	1.933	0.494	3.234	0.844	1.523

Coeff. $|C_i| \times 10^{-2}$	f_5=100 Hz					f_6=120 Hz				
	C_0	C_1	C_2	C_3	C_4	C_0	C_1	C_2	C_3	C_4
Uncloaked voids	0.210	0.511	5.749	0.420	2.363	4.214	3.529	3.608	3.000	3.413
Cloaked voids	0.110	0.285	1.032	0.464	2.103	2.326	1.901	1.005	1.431	1.736

Coeff. $|C_i| \times 10^{-2}$	f_7=140 Hz					f_8=160 Hz				
	C_0	C_1	C_2	C_3	C_4	C_0	C_1	C_2	C_3	C_4
Uncloaked voids	1.052	4.580	1.803	4.781	0.325	2.161	0.870	4.792	0.428	1.708
Cloaked voids	0.676	2.952	0.297	3.275	0.289	1.094	0.512	0.740	0.089	0.443

Coeff. $|C_i| \times 10^{-2}$	f_9=180 Hz					f_{10}=200 Hz				
	C_0	C_1	C_2	C_3	C_4	C_0	C_1	C_2	C_3	C_4
Uncloaked void	3.930	0.051	7.186	0.241	22.518	1.677	2.379	29.040	0.288	73.118
Cloaked void	3.072	0.043	0.920	0.054	9.379	0.587	1.496	8.671	0.182	21.385

Tab. 1: Absolute value of the Fourier Coefficients $|C_i|$ evaluated along the circle path of radius R_1=130 mm for different flexural vibrations of frequencies f_1=20 Hz, f_2=40 Hz, f_3=60 Hz, f_4=80 Hz, f_5=100 Hz, f_6=120 Hz, f_7=140 Hz, f_8=160 Hz, f_9=180 Hz, and f_{10}=200 Hz, corresponding to the data reported in Figs. 5 and 6. Results show that the moduli of the Fourier coefficients for the case of the cloaked void are smaller than those referring to the case of uncloaked void.

Coeff. $\|C_i\| \times 10^{-2}$	f_1=20 Hz					f_2=40 Hz				
	C_0	C_1	C_2	C_3	C_4	C_0	C_1	C_2	C_3	C_4
Uncloaked voids	0.016	2.628	1.996	0.477	0.115	2.126	0.132	6.277	0.127	1.637
Cloaked voids	0.066	1.295	0.838	0.263	0.050	0.515	0.087	0.817	0.071	0.317

Coeff. $\|C_i\| \times 10^{-2}$	f_3=60 Hz					f_4=80 Hz				
	C_0	C_1	C_2	C_3	C_4	C_0	C_1	C_2	C_3	C_4
Uncloaked voids	0.152	2.715	0.187	17.964	0.473	3.982	2.725	6.879	1.916	5.205
Cloaked voids	0.216	0.991	0.236	8.055	0.480	1.447	1.364	2.074	0.966	2.145

Coeff. $\|C_i\| \times 10^{-2}$	f_5=100 Hz					f_6=120 Hz				
	C_0	C_1	C_2	C_3	C_4	C_0	C_1	C_2	C_3	C_4
Uncloaked voids	1.195	0.255	4.854	0.331	3.103	2.456	3.571	1.132	2.223	3.865
Cloaked voids	0.878	0.087	0.774	0.432	2.750	1.439	1.828	0.113	1.158	1.973

Coeff. $\|C_i\| \times 10^{-2}$	f_7=140 Hz					f_8=160 Hz				
	C_0	C_1	C_2	C_3	C_4	C_0	C_1	C_2	C_3	C_4
Uncloaked voids	1.048	3.611	1.416	3.406	0.304	3.309	1.521	5.260	0.417	1.654
Cloaked void	0.742	2.459	0.127	2.178	0.286	2.514	0.908	0.068	0.086	0.442

Coeff. $\|C_i\| \times 10^{-2}$	f_9=180 Hz					f_{10}=200 Hz				
	C_0	C_1	C_2	C_3	C_4	C_0	C_1	C_2	C_3	C_4
Uncloaked voids	1.932	0.867	7.576	0.367	18.272	29.363	0.992	50.335	0.733	52.025
Cloaked voids	1.113	0.513	1.882	0.070	7.399	7.632	0.559	17.428	0.077	15.169

Tab. 2: Absolute value of the Fourier Coefficients $|C_i|$ evaluated along the circle path of radius R_2=150 mm for different flexural vibrations of frequencies f_1=20 Hz, f_2=40 Hz, f_3=60 Hz, f_4=80 Hz, f_5=100 Hz, f_6=120 Hz, f_7=140 Hz, f_8=160 Hz, f_9=180 Hz, and f_{10}=200 Hz, corresponding to the data reported in Figs. 5 and 6. Results show that the moduli of the Fourier coefficients for the case of the cloaked void are smaller than those referring to the case of uncloaked void.

3.4 Concentrated mass model versus smeared mass model

In the reinforcement of the structured plate, the mass redistribution has been assumed as discrete in the previous sections, but a continuous redistribution is also possible, and the result is almost unchanged. The situation in which the mass density is uniformly increased along the boundary of the square void is explored below. Although the two cases of discrete and diffused redistribution of mass are in essence different, it is shown that the two models display almost identical behaviours. In particular, computations have been performed, in which the additional masses placed at the boundary nodal points as shown in Fig. 7, have been redistributed uniformly along the boundary ligaments of the square void. The comparative results for the scattered flexural displacements in the two cases of the discrete and continuous redistribution of the mass in a layer placed along the boundary of the
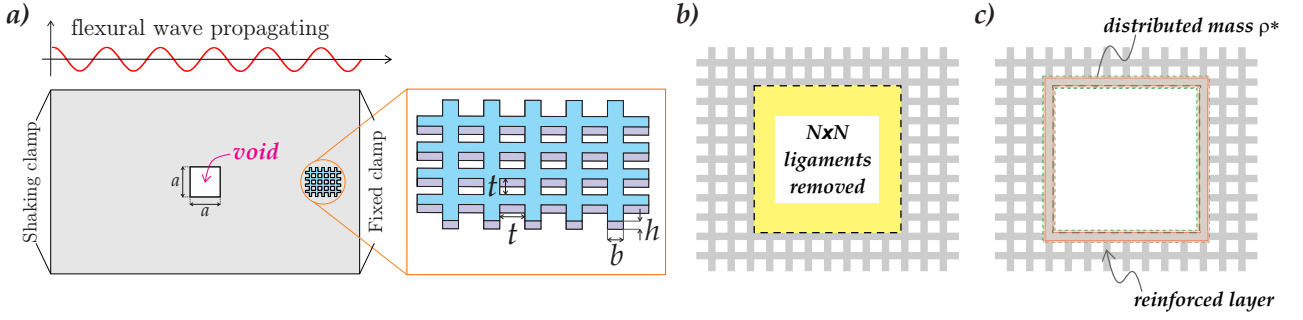
void are shown in Figs. 8 and 9.

Fig. 7: (a) Flexural lattice with a square void. (b) Intact flexural lattice. (c) A lattice with the square void cloaked with a continuous layer of reinforcement, so that mass and stiffness are uniformly redistributed.
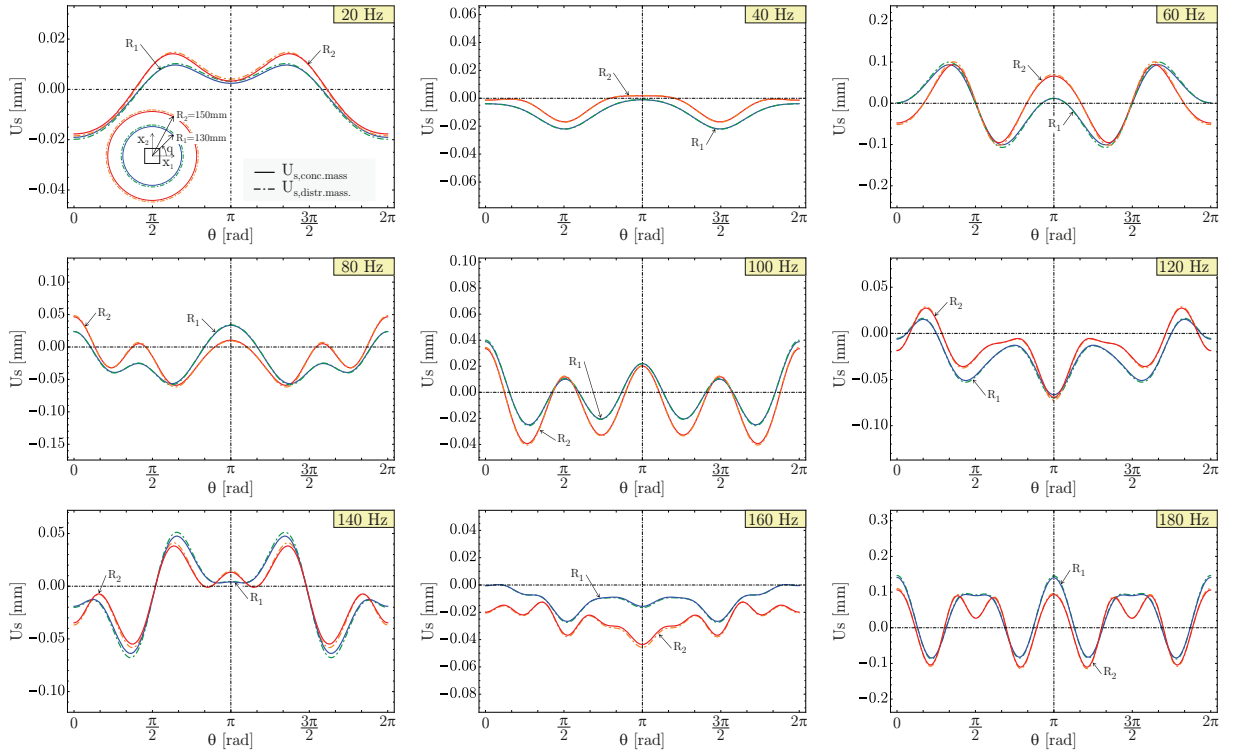

Fig. 8: Comparison between the scattered fields, evaluated along two concentric circles (blue/green for radius 130 mm and red/orange for 150 mm), for the structured plate containing the reinforced square void in the case of a concentrated mass redistribution (continuous lines) and in the case of uniform mass redistribution. The difference in the scattered fields for the two mass redistributions models is insignificant.
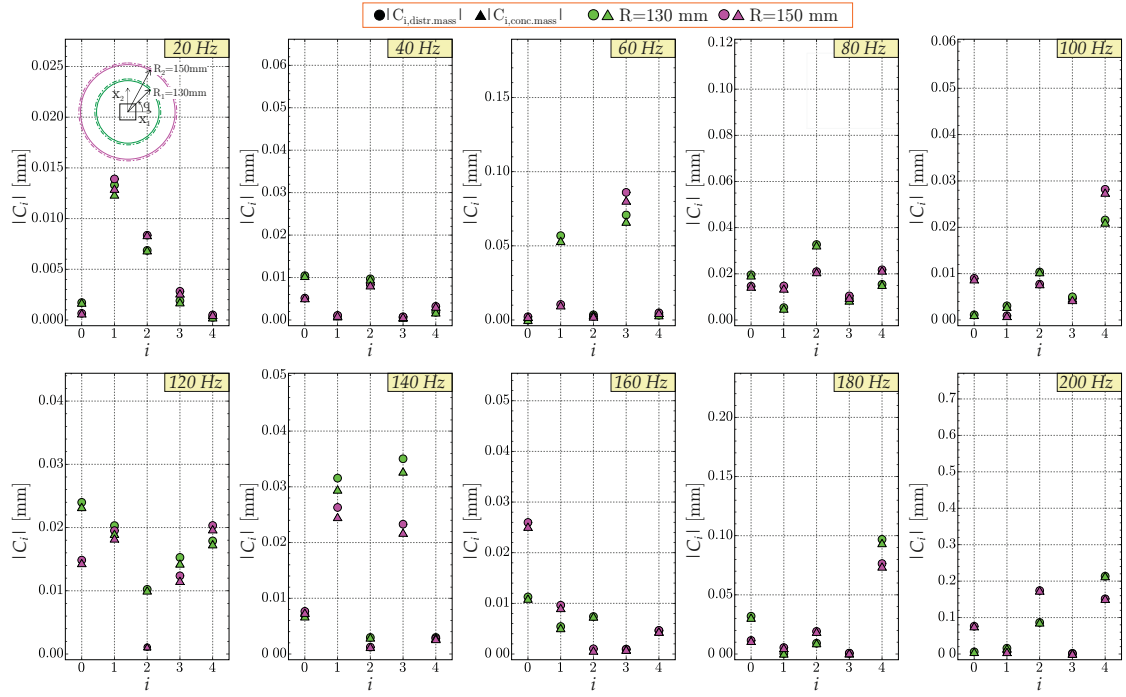
Fig. 9: As for Figs. 5 and 6, but now two systems of reinforcement are compared, namely, cloaking realized with a discrete reinforcement and concentrated mass distribution (circular spots) and with a continuous layer of equivalent stiffness and mass (triangular spots). The results show excellent agreement between the two cloaking systems (discrete and continuous distribution of an additional mass) for the chosen frequency range.

References

[1] Sanchis L, Garcia-Chocano VM, Llopis-Pontiveros R, Climente A, Mart´inez-Pastor J, Cervera F, Sánchez-Dehesa J. 2013 'Three-Dimensional Axisymmetric Cloak Based on the Cancellation of Acoustic Scattering from a Sphere.' *PRL*, **110**, 124301.

[2] Chen Y, Xiaoning L, Gengkai H. 2015 'Latticed pentamode acoustic cloak', *Sci. Rep.*, **5**, 15745.

[3] Norris AN, Shuvalov AL. 2011 'Elastic cloaking theory', *Wave Motion*, **48**, 525-538.

[4] Brun M, Guenneau S, Movchan AB. 2009 'Achieving control of in-plane elastic waves' *Appl. Phys. Lett.*, **94**, 061903.

[5] Norris AN. 2008 'Acoustic cloaking theory.' *Proc. R. Soc. A*, **464**, 2411-2434.

[6] Jones IS, Brun M, Movchan NV, Movchan AB. 2015 'Singular perturbations and cloaking illusions for elastic waves in membranes and Kirchhoff plates', *Int. J. Solids Structures*, **69-70**, 498-506.

[7] Norris AN, Parnell WJ. 2012 'Hyperelastic cloaking theory: Transformation elasticity with pre-stressed solids', *Proc. R. Soc. A*, **468**, 2146.

[8] Brun M, Colquitt DJ, Jones IS, Movchan AB, Movchan, NV. 2014 Transformation cloaking and radial approximations for flexural waves in elastic plates. *New J. Phys.*, **16**, 093020.

[9] Colquitt DJ, Brun M, Gei M, Movchan AB, Movchan NV, Jones IS. 2014 Transformation elastodynamics and cloaking for flexural waves. *J. Mech. Phys. Solids*, **72**, 131-143.

[10] Farhat M, Guenneau S, Enoch S. 2012 'Broadband cloaking of bending waves via homogenization of multiply perforated radially symmetric and isotropic thin elastic' *Phys. Rev. B*, **85**(2), 020301.

[11] Stenger N, Wilhelm M, Wegener M. 2012 'Experiments on Elastic Cloaking in Thin Plates', *Phys. Rev. Letters*, **108**, 014301.

14

[12] Xingjie N, Wong ZJ, Mrejen M, Wang Y, Zhang X. 2015 'An ultrathin invisibility skin cloak for visible light.' *Science*, **349**(6254), 1310-1314.

[13] Bückmann T, Thiel M, Kadic M, Schittny R, Wegener M. 2014 An elasto-mechanical unfealability cloak made of pentamode metamaterials. *Nat. Commun.*. **5** 4130.

[14] Bückmann T, Kadic M, Schittny R, Wegener M. 2015 'Mechanical cloak design by direct lattice transformation', *PNAS*, **112** (16), 4930-4934.

[15] Parnell WJ. 2012 'Nonlinear pre-stress for cloaking from antiplane elastic waves', *Proc. R. Soc. A*, **468**, 563-580.

[16] Parnell WJ, Norris AN, Shearer T. 2012 'Employing pre-stress to generate finite cloaks for antiplane elastic waves', *Appl. Phys. Lett.*, **100**, 171907.

[17] Darabi A, Zareei A, Alam MR, Leamy MJ. 2018 Experimental Demonstration of an Ultrabroadband Nonlinear Cloak for Flexural Waves. *Phys. Rev. Lett.*, **121**, 174301.

[18] Colquitt DJ, Jones IS, Movchan NV, Movchan AB, Brun M, McPhedran RC. 2013 Making waves round a structured cloak: lattices, negative refraction and fringes. *Proc. R. Soc. A*, **469**, 20130218.

[19] Misseroni D, Colquitt DJ, Movchan AB, Movchan NV, Jones IS. 2016 Cymatics for the cloaking of flexural vibrations in a structured plate. *Sci. Rep.*, **6**, 23929.

[20] Farhat M, Guenneau S, Enoch S, Movchan AB. 2009 'Cloaking bending waves propagating in thin elastic plates', *Phys. Rev. B*, **79**, 033102.

[21] Fleury R, Alù A. 2014 'Cloaking and invisibility: A review, *Forum for Electromagnetic Research Method and Applications Technologies (FERMAT)*, vol.1, no. 9.

[22] Schurig D, Mock JJ, Justice BJ, Cummer SA, Pendry JB, Starr AF, Smith DR. 2006 Metamaterial electromagnetic cloak at microwave frequencies. *Science*, **314**, 977980.

[23] Liu R, Ji C, Mock JJ, Chin JY, Cui TJ, Smith DR. 2008 'Broadband ground-plane cloak', *Science*, **323**, 366 (2008).

[24] Nathan L, Smith DR. 2013 'A full-parameter unidirectional metamaterial cloak for microwaves.' *Nat Rev Mater*, **12**, 25-28.

[25] Milton GW, Briane M, Willis JR. 2006 On cloaking for elasticity and physical equations with a transformation invariant form. *New J. Phys.*, **8**, 248.

[26] Guenneau S, McPhedran, RC, Enoch S, Movchan AB, Farhat M, Nicorovici NAP. 2010 The colours of cloaks. *J. Opt.*, **13**, 024014.

[27] Farhat, M, Chen, PY, Bağci H, Enoch S, Guenneau S, Alu A. 2014 Platonic Scattering Cancellation for Bending Waves in a Thin Plate. *Sci. Rep.*, **4**, 4644.

[28] Brûlé S, Javelaud EH, Enoch S, Guenneau S. 2014 'Experiments on Seismic Metamaterials: Molding Surface Waves', *Phys. Rev. Lett.*, **112**, 133901.

[29] Achaoui Y, Antonakakis T, Brûlé S, Craster RV, Enoch S, Guenneau S. 2017 Clamped seismic metamaterials: Ultra-Low Broad Frequency stop-bands. *New J. Phys.*, **19**, 063022.

[30] Miniaci M, Krushynska A, Bosia, F, Pugno NM. 2016 'Large scale mechanical metamaterials as seismic shields.' *New J. Phys.*, **18** 083041.

[31] Timoshenko S, Woinowsky-Krieger S. 'Theory of plates and shells', McGraw-Hill Book Company.